ACCSCIENCE PUBLISHING

Artificial Intelligence in Health

ORIGINAL RESEARCH ARTICLE

Artificial intelligence in cardiac rhythm diagnostics and management: Challenges and opportunities

Robert Splinter[1,2,3,4]*

[1]Intelligent Bioinformatics Ltd, Thirsk, North Yorkshire, United Kingdom

[2]Intelligent Bioinformatics LLC, Mooresville, North Carolina, United States of America

[3]Departments of Physics and Optical Science, University of North Carolina at Charlotte, Charlotte, North Carolina, United States of America

[4]Departments of Mathematics and Statistics, University of North Carolina at Charlotte, Charlotte, North Carolina, United States of America

Abstract

Each day, one million people undergo electrocardiogram diagnostics. The diagnostic process is time-consuming and often yields incomplete or inconclusive results, placing significant strain on physicians. Artificial intelligence (AI)-assisted diagnosis can significantly alleviate this burden by enhancing diagnostic accuracy and efficiency, and its application is gaining traction across various fields. With the increasing number of patients and a growing backlog of diagnostic appointments, AI can offer physicians benefits such as accurate, timely, and reliable assistance in reviewing vital signs and conducting physical examinations for individual patients. As physicians face mounting pressure from insurance companies and government guidelines for consultation time, AI can help streamline the diagnostic process. In particular, with the growing global attention on cardiac health (and the overall decline thereof), the range of automated diagnostic opportunities is expanding rapidly. Additional mathematical processing tools can provide probabilistic assessments of various cardiac conditions, reducing physicians' workload while enhancing treatment options. AI has already demonstrated success in expediting the detection of pathological cardiac depolarization abnormalities and shortening diagnostic time frames. However, AI-based diagnostics requires further validation and safeguards to minimize diagnostic inaccuracies, ensuring its reliability and safety in clinical practice.

Keywords: Machine learning; Diagnostics; Medicine; Risk stratification; Screening; Signal-processing; Matched filter; Wavelet analysis

***Corresponding author:**
Robert Splinter
(rsplinter@ibi-gb.com)

Citation: Splinter R. Artificial intelligence in cardiac rhythm diagnostics and management: Challenges and opportunities. *Artif Intell Health*. 2025;2(3):107-124. doi: 10.36922/aih.8468

Received: January 9, 2025

Revised: March 3, 2025

Accepted: March 12, 2025

Published online: April 2, 2025

1. Introduction

Data from four large population-based registries, which contain emergency medical service data collected between 2012 and 2017 across major European Union (EU) countries, report at least 450,000 cases of sudden cardiac death (SCD) annually.[1] Similarly, heart failure poses a significant economic burden on the United States (US),

with costs projected to reach US $70 billion by 2030. The cost of heart failure varies widely, from less than US $1,000 per patient in low-income countries to €5,000 – 15,000 in Europe and US $17,000 – 30,000 in the US. Accurate and timely diagnostic screening, coupled with advanced warning systems, could save approximately 1,250 lives per day in the US, 40 in the United Kingdom (UK), and 1,100 across the EU. Notably, data from Asia and Russia remain incomplete. SCD, often caused by ventricular fibrillation (VF), affects individuals of all ages, depending on factors such as congenital disorders and lifestyles. The incidence in pediatric and juvenile populations can be as high as 1 in 10,000. Women are generally disproportionately affected and often face underdiagnoses or misdiagnoses. In addition, people of African descent and Asian Indian men are more frequently affected than Caucasians. The use of AI in medical diagnostics can save time, enhance the level of detail, and improve early detection of pathological conditions. It can uncover warning signs of deviations in the image and signal patterns that may require follow-up investigations and potentially additional tests.[2-7]

The limitations of manual analysis of diagnostic results include personal preferences, bias, high dependency on professional experience, skills, and abilities, and personal health conditions, such as fatigue, eyesight problems, and personal medical history (e.g., color blindness). For example, traditional X-ray imaging alone may fail to fully assess coronary stenoses or predict the progression of life-threatening cardiovascular conditions. One important characteristic of coronary health, particularly cardiac depolarization health, is the recognition of fatal factors underlying disease progression. AI-driven computational analysis can enhance pattern recognition and identify clusters of subtle abnormalities that may be overlooked by visual inspection, such as those in peak-to-peak sequencings and groupings like image-clustering.[8-11]

One area of interest in diagnostics that may benefit from automated screening through software algorithms, often mathematically based, is electrocardiogram (ECG, also known as electrocardiogram in German) acquisition. The ECG was introduced in 1903 by Willem Einthoven from the Netherlands, who pioneered the use of a specially designed galvanometer to record the action potentials. Early recordings were obtained by immersing hands and feet in saltwater to enhance conductivity. The ECG captures the electrical depolarization and repolarization of cardiac muscle cells.[12,13] These electrical signals, known as action potentials, result from the flow of ions across the cell membrane, leading to muscle contraction. A single ECG cycle is illustrated in Figure 1A, while a representative healthy ECG is shown in Figure 1B. The ECG waveform typically consists of five distinct peaks labeled P, Q, R, S, and T, with a frequently observed sixth peak, the U wave. The P wave is the result of the depolarization of the atria, while the remaining waves are caused by the depolarization of the ventricles. The R wave represents the synchronized depolarization of the right and left ventricles over time.

Cardiac muscles contract as a direct result of cellular electrical excitation, mediated by active and passive ion transport across cell membranes. Cardiac cells are not directly stimulated by neurons but instead initiate depolarization through an intrinsic excitation process. The depolarization of one cell triggers a cascade of depolarization and contraction in neighboring cells, resulting in coordinated atria and ventricular contractions that pump blood through the heart. The electrical activation of each cardiac cell serves as an indication of its health and functional state. The summation of these electrical activities can be represented as a vector, which changes direction as depolarization propagates through the heart (Figure 2). The details of this vector rotation can be captured by placing multiple electrodes on the skin.

Modern ECG systems employ advanced signal processing techniques to enhance the signal-to-noise ratio, enabling precise analysis of arrhythmogenic tendencies. The ECG is, therefore, the cumulative result of the depolarization of individual cardiac muscle cells over time, occurring in a controlled and repetitive manner. The 12-lead ECG, the most detailed configuration, offers spatial information about depolarization patterns over time (Figure 3). In contrast, most other detection and monitoring techniques only provide temporal information. By recording the depolarization of cardiac muscle cells over extended periods, clinicians can diagnose abnormalities, identify malfunctioning regions, and determine the need for further medical intervention. Deviations from a typical ECG pattern, whether detected visually or through signal processing, can be classified as specific cardiac disorders. During VF, the depolarization vector will no longer be recognizable due to the random and chaotic nature of electrical activity in the ventricles.[9,10,14,15]

This paper introduces the pathological conditions that can potentially be identified using various mathematical techniques under AI-driven signal processing. Each condition may require unique technical approaches. The ultimate goal is to provide predictive mechanisms for early detection and prevention of cardiac disorders. The early detection and intervention of cardiac disorders require a highly regulated control system, which is currently under development and may take several years for market release. It is important to recognize that AI-based diagnosis is not a standalone solution. Medical screening requires a

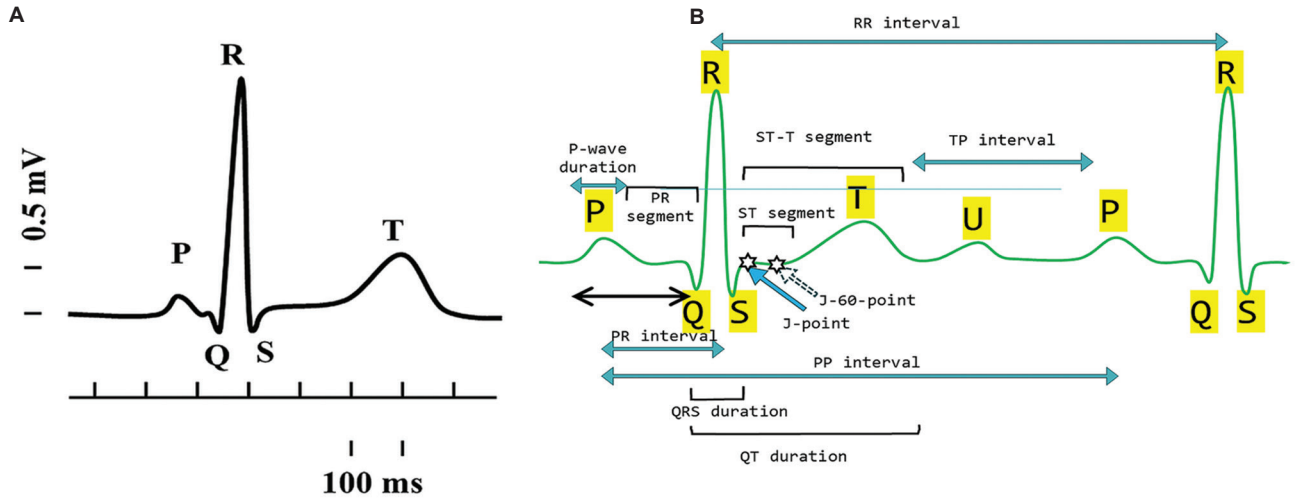

Figure 1. Synopsis of the representative and essential components in the electrocardiogram recording. (A) A standard single-period heartbeat depolarization pattern illustrates atrial depolarization (P), the ventricular depolarization sequence (QRS complex), and ventricular repolarization (T), followed by a possible U wave, representing the final phase of ventricular repolarization. Prominent U waves are characteristic of hypokalemia. (B) Heart depolarization intervals and critical markers. The PR interval typically ranges from 0.12 to 0.22 s. The QRS complex duration in a healthy person is generally <0.12 s. The J-point serves as a reference for detecting ST segment elevation or depression. The J-60 point is used to assess ST segment depression, particularly during exercise stress testing. The QT interval varies between males and females. In healthy adults, the QT interval is generally <0.45 s for males and <0.47 s for females. For calibration, the PR segment provides the most relevant baseline and isoelectric level information. The PR segment level is crucial for accurately determining ST-segment elevation or depression.

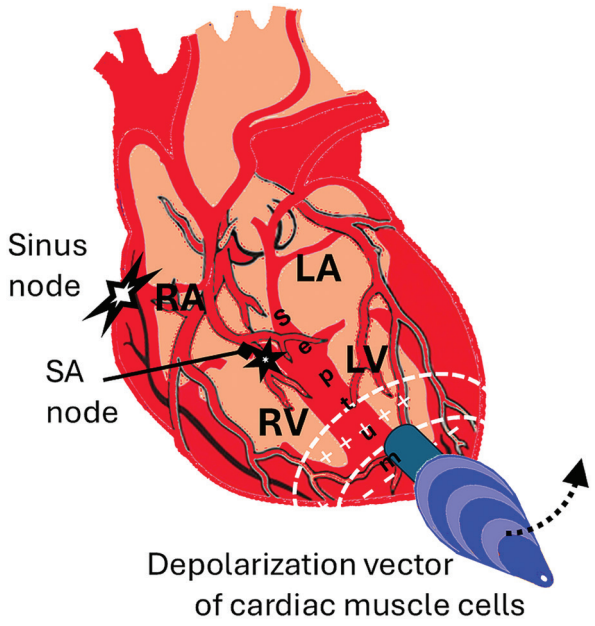

Figure 2. Representative illustration of the depolarization vector rotating through three-dimensional space during a cardiac beat (P-QRS), facilitating organized contraction.
Abbreviations: LA: Left atrium; LV: Left ventricle; RA: Right atrium; RV: Right ventricle; SA: Sinoatrial.

multidisciplinary approach that accounts for individual variability in vital signs, psychosomatic modulation (e.g., the white coat syndrome, infatuation, fear, and anxiety), and biochemical interactions. Although AI can provide recommendations for potential diagnostic conclusions and estimate the probabilities of various pathological conditions identified through mathematical models, the final diagnosis remains the responsibility of the attending physician.

2. Background

Accurate, rapid, and reliable diagnostics and patient care fundamentally depend on the integration of biochemical and physiological information obtained from various sources through multiple techniques. The acquisition and computerized processing of as much relevant information as possible, for instance, using AI, will enhance diagnostic precision and facilitate the development of effective and reliable treatment regimens.[8] Access to a patient's complete medical history is crucial in a diagnosis, as is the ability to compare the patient's data against known pathological patterns from a broad population database. Such comparisons enable early screening, identification of health conditions, and determination of the most appropriate treatment modalities or the need for additional follow-up tests targeting specific physiological, anatomical, or biochemical factors. Equally important is the ability to situate the patient within the appropriate segment of the statistical distribution relevant to their suspected pathology. Even for the same individual, physiological values can vary significantly due to factors such as activity levels, time of day

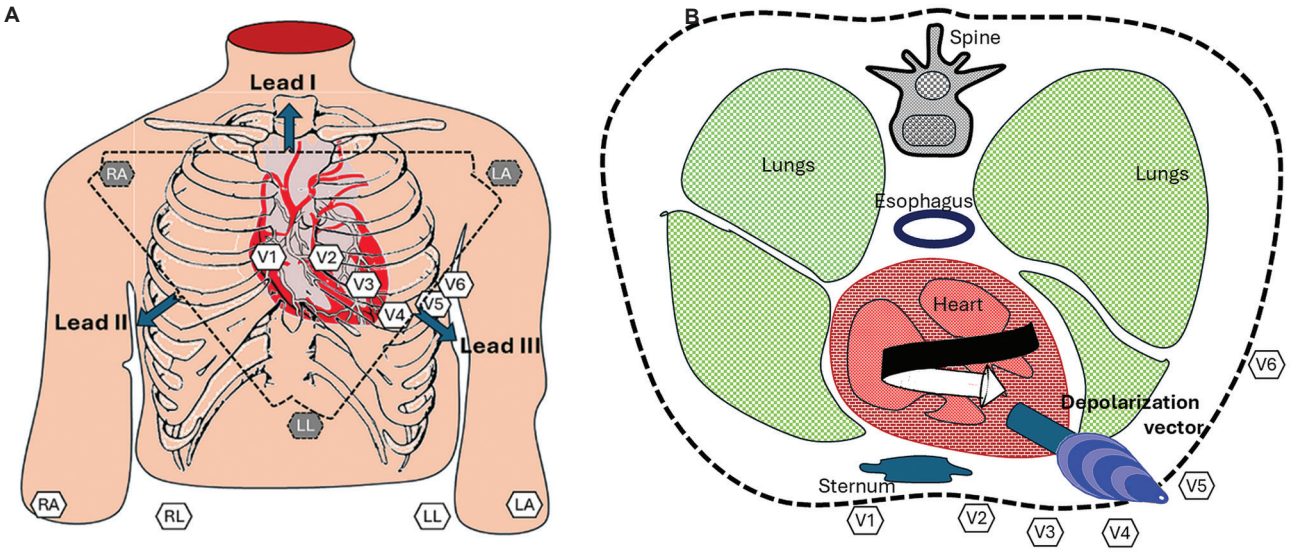

Figure 3. Typical placement of leads in a 12-lead electrocardiogram. (A) Coronal (frontal) view. (B) Axial (transverse) view
Abbreviations: LA: Left arm; LL: Left leg; RA: Right arm; RL: Right leg; V1: 4th intercostal space, right margin of the sternum; V2: 4th intercostal space, left sternal edge; V3: Midpoint between V2 and V4; V4: 5th intercostal space, midclavicular line (symmetrically opposed to V2; V5: Anterior axillary line; V6: Midaxillary line, forming a straight line with V4 and V5.

(e.g., morning vs. evening), gender (e.g., male vs. female), hormonal status, emotional state (e.g., aggression), and other boundary conditions. Anatomical deviations further complicate diagnostics. For example, while over 99% of the population has a heart located on the left side of the chest, a small minority (<1%) exhibit dextrocardia, where the heart is located on the right side.[16-18] This anatomical anomaly has profound implications for diagnostic imaging and interpretation. For instance, a chest X-ray of a patient with dextrocardia will appear markedly different from the norm. Similarly, the analysis based on a 12-lead ECG will deviate significantly from conventional patterns: the R wave amplitude in electrodes V1 through V6 will be diminished, and the P wave, QRS complex, and T wave will appear inverted in leads I and augmented vector left, as illustrated in Figure 4.

The variability in data between individuals, as well as within the same individual under different conditions, underscores the importance of verifying and validating preliminary diagnoses through multiple approaches, such as follow-up examinations, professional expertise in root-cause analysis, and consideration of personal history (including genetics) of the patient and the associated patient cohort. Another important diagnostic aspect is risk stratification, which assesses the severity of the patient's condition and determines the urgency of therapeutic intervention. Cardiovascular disease represents a financial burden, costing the EU €282 billion annually.[19] In 2022 alone, general cardiac-related healthcare and long-term medical support accounted for €155 billion. Cardiac health costs the EU 11% of its health budget. Furthermore, productivity losses add in an additional €48 billion, while the costs for out-of-hospital expenses, including in-home support, contribute an additional €79 billion each year – a figure that continues to grow.

3. Methods

In this article, examples of the application of decade-old AI in diagnostics, focusing on signal processing techniques, are described, along with more recent advancements. Some of the AI applications may not solely rely on software techniques. Here, some recent feasibility and pilot diagnostic stages of discovery are also discussed, though, due to the early stage of exploration and proprietary considerations, not all developmental stages are discussed. At this exploratory stage, no claims can be made regarding the accuracy and reliability of these AI-driven diagnostic tools for identifying certain pathological cardiac rhythm disorders. All diagnostic outcomes were compared against documented disorders in the data files and physician reviews. However, given the limited scope of conditions examined and the preliminary nature of the research, a comprehensive statistical validation is not yet feasible. It is important to note that AI-backed diagnostic systems fall under the classification of Class IIb medical devices, which mandates rigorous statistical analysis, including extensive animal and human trials. No animal or human trials have been conducted at this point. The long-term development of these medical device applications is part of a greater corporate plan.

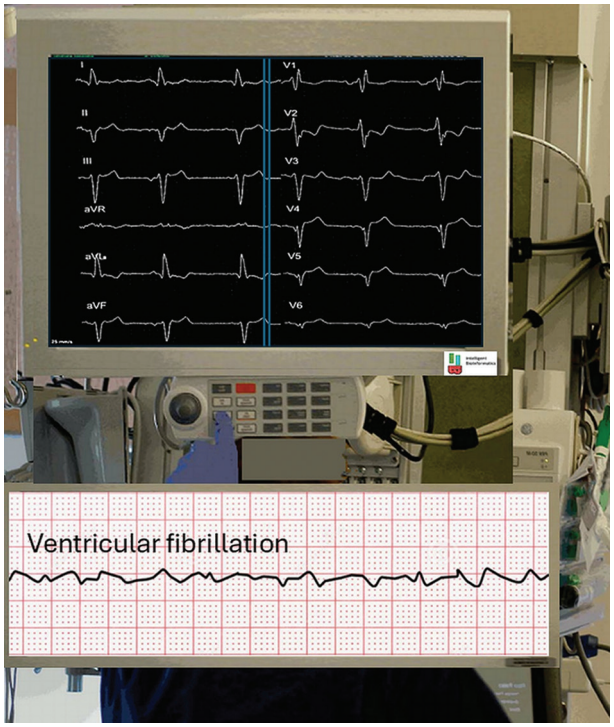

Figure 4. Representation of the acquired 12-lead electrocardiogram recordings: V1, V2, V3, V4, V5, V6, I, II, III, augmented vector right (aVR), augmented vector left (aVL), augmented vector foot (aVF). The bottom section illustrates the complete lack of signal cohesion in ventricular fibrillation. Recording locations: V1: Refer to Figure 3; V2–V4: Record from the front of the heart and are the anterior leads; V5 and V6: Record from the left side of the heart and are the lateral leads; Lead I (bipolar): Between aVL and aVR, creating a second high lateral lead; Lead II (bipolar): Between aVR and aVF, generating the second inferior lead; Lead III (bipolar): Between aVL and aVF, generating the third inferior lead; aVF: Left ankle or left lower abdomen; aVL: Left wrist or shoulder; aVR: Right wrist or shoulder.

All data processing for this research is conducted using high-end personal computers. While some of these analytical procedures can be programmed into existing approved monitoring devices, more complex approaches, such as wavelet and matched filter techniques, require specialized programming adjustments for use in standalone clinical monitoring devices. Notably, no final clinical solutions are provided at this point.

3.1. Programming and its mechanisms

Various programming languages are used to achieve diagnostic modalities and protocols. The input signal is often managed using various mathematical techniques, including noise reduction, filtering, feature extraction, and compression. Examples of the programming languages being used are Machine Language, C, C++, Java, Python, R, Structured Query Language, Swift, MatLab, and Perl. The choice of programming language is often determined by processing speed, convenience of data routing, and the implementation of higher mathematical techniques whenever necessary for complex signal processing. Examples of signal processing mechanisms are the Fourier transform, wavelet transform, Wiener filter, Kalman filter, whitening filter, Butterworth filter, Whiterock filter, whitening transformation, and matched filter processing.[19-28] While a majority of these processing tools are applied in signal denoising techniques, others have more specific tasks in pattern recognition, particularly isolated pathological deviations in an individual's ECG signal. Analog-based signal processing techniques, such as frequency cutoffs (low-pass, high-pass, and band-pass filtering), can be implemented using electronic hardware and computationally, often in conjunction with Fourier transform processing. In machine learning applications, neural networks are used to acquire signals and generate screening templates that represent various pathological conditions. However, significant work remains in defining these templates and customizing them for individual patients. With more than 50 cardiac conditions to consider, distinguishing risk factors and electrophysiological characteristics presents a significant challenge.

Diagnostic screening is further complicated by the stringent confidence levels required for Class IIb medical devices. The infrequency of certain arrhythmogenic episodes adds another layer of complexity, necessitating careful selection of start and end times for the data stream used for the creation of analytical templates. Automated selection of these time frames can be achieved using neural network processing and other signal-processing techniques, such as identifying deviations from established reference depolarization patterns by omitting peaks at specific temporal locations. These computational procedures are integral to the broader toolkit of AI-driven neural network processing. In most cases, analog-to-digital conversion is required before automated signal processing can be performed. Various off-the-shelf analog-to-digital converters are available to perform this task electronically, enabling digital signal processing. Analog signal processing, on the other hand, includes traditional techniques, such as signal amplitude control, modulation/demodulation (e.g., frequency modulation and amplitude modulation), and a plethora of electronic error correction techniques.

3.2. Signal processing: a theoretical approach to the determination of depolarization pattern

An important temporal feature in ECG analysis is the duration of the QRS complex, which is typically identified by its characteristic shape and relatively stable time constant within the waveform. Another critical feature is

the time interval between the T wave and the subsequent P wave. This measure is important because it reflects the separation between two key cardiac events, that is, the excitation pulse from the sinus node, represented by the P wave, and the repolarization of the ventricles, which generates the T wave.

To successfully capture and analyze various cellular depolarization frequency patterns, multiple signal processing approaches can be employed, including analog processing, digital signal processing, or a mixed signal processing format. Other techniques include peak detection, frequency determination, the time interval between specific peaks analysis (either same function or different function [Figure 2]: e.g., QT separation, QQ separation, and P-wave repetition rate [which can indicate atrial fibrillation]), pulse widths of various components in the PQRST complex analysis, wavelet transform (however limited due to the temporal nature of pacing events), discrete wavelet transform, Butterworth filtering, discrete path transform, Fourier transform, short-term Fourier transform, Laplace signal transform, and compressed or full matched filter analysis.

Time constants, such as heart rate and various interval period durations (e.g., PR interval, QT interval, and P-wave repetition rate), can be efficiently determined using peak detection or Fourier transform techniques. These computational methods are applicable to any ECG data acquisition system. Notably, peak detection and heart rate variability tests are decade-old techniques that have been used in standard monitoring devices.

For preliminary analyses, various data banks containing healthy and pathological ECG recordings are available, such as those hosted on PhysioNet (https://physionet.org/). Collaborations with cardiology groups have also yielded highly specific data streams. All analytical signals in this study were acquired using routine clinical monitoring equipment. Some analyses were conducted as single-blinded studies, where the analytical team was provided with a well-established arrhythmogenic signal without knowing that it was abnormal. The physicians supplying the signals were fully aware of the deviations, which were often clearly defined. However, due to the early stages of development, not all hidden characteristics and atypical ECG patterns have been investigated for diagnostic purposes at this time.

3.3. Signal analysis in amplitude, temporal framework, spatial framework, and frequency spectrum

Various approaches are employed to evaluate the temporal aspect of ECG signals, such as peak-to-peak analysis, amplitude variability within specific time frames, durations and intervals between sequences of events, and correlation analysis between signals or between certain variables. The most critical temporal feature in ECG analysis is the heart depolarization cycle period, which is determined by measuring the duration from one R wave to the next. Other important features include the duration of individual waves and the time interval between them (e.g., the TP interval: time interval between the T and P waves). The TP interval is important because it reflects the separation between two important events, that is, the pulse rate of the sinus node, which is represented by the P wave, and the ventricular repolarization, which generates the T wave. A broad range of signal processing techniques, applicable in the time and frequency domains, are summarized in Table 1.[11,29-34] While it is beyond the scope of this article to discuss each of these techniques, they can be utilized for different purposes, such as signal pre-processing, noise reduction, and identifying the pathological origins of signal deviations. For instance, unique, idiosyncratic, or infrequent deviations from the normal ECG pattern may be detected using specialized approaches like modified matched filter analysis. The spatial domain is particularly significant in 12-lead ECG and multidimensional decomposition techniques, such as the matched filter approach.

Various standard ECG characteristics can be resolved using straightforward mathematical techniques. For instance, peak detection can quickly determine heart rate, while wavelet transform and matched filter approaches can define specific intervals and segments in the time domain (Figure 1). However, due to continuous advancements in signal processing and innovative approaches, it is impossible to cover all mechanisms within this article. Peak detection results related to the time domain can also be used for the recognition of certain arrhythmias. Besides, atrial and VF require a more complex mathematical approach for early and proactive detection.

An important time-domain feature in ECG is the duration of the QRS complex. In general, the QRS complex is identified by its characteristic shape and relatively stable time constant within the repetitive ECG pattern. In terms of frequency content, the ECG waveform, including the QRS complex, is primarily confined to the high-frequency region, while the P and T waves represent the lower-frequency components. The ST segment, on the other hand, is time-restricted and characterized by its low-frequency content.[8]

The frequency content of a normal ECG often differs significantly from that of a pathological ECG. For instance, a normal heart rate ranges between 60 and 100 beats/min, whereas arrhythmias or fibrillation can result in heart rates

Table 1. Overview of common temporal and frequency analysis tools

Time domain	Frequency domain
Analog-to-digital conversion	Adaptive filtering
Amplitude	Band-pass filtering
Autoregressive model	Continuous wavelet transform
Bilinear transform	Convolution
Continuous	Correlation
Convolution	Discrete cosine transform
Correlation	Discrete Fourier transform
Discrete	Empirical mode decomposition
Discriminant functions (least squares/synthetic)	Fast Fourier transform
Duration	Finite impulse response filtering
Event analysis (missing events)	Fourier transform
Finite impulse response filtering	High-pass filtering
Infinite impulse response filtering	Infinite impulse response filtering
Interval	Inverse Fourier transform
Least squares discriminant functions	Laplace transform
Least squares method (in time series)	Least-squares discriminant analysis
Matched filter technique	Least-squares wavelet analysis
Recurring sequence of events	Low-pass filtering
Sampling property of unit impulse	Matched filter techniques
Synthetic discriminant functions	Phase-shift analysis
Time-reversal technique	Sampling (e.g., Nyquist–Shannon sampling theorem), analog-to-digital conversion
Trigger point	Spectral confinement
Wavelet transform	Spectral decomposition
Z-transform	Synthetic discriminant functions
	S-transform
	Wavelet transform
	Windowing
	Z-transform

Notes: Some specific frequency filters: Wiener filter, Kalman filter, whitening filter, Butterworth filter, Whiterock filter, and whitening transformation; [11] All diagnostic modalities are represented in no particular order, alphabetically ranked.

exceeding 200 beats/min. It is worth noting that a teenager engaged in sporting activities may easily reach or exceed a heart rate of 240 beats/min without immediate health concerns. Beyond differences in heart rate, depolarization and repolarization (on- and off-ramps) can be altered under pathological conditions, requiring an extensive analytical frequency bandwidth to accurately capture these variations in the frequency domain.[8]

In the Fourier domain, a standard (healthy) ECG can be accurately described using the first eight harmonics of the heart rate. However, even minor high-frequency deviations from the conventional ECG waveform often introduce alterations, requiring a larger number of higher harmonics to characterize the frequency-domain features. The baseline ECG typically has a root frequency of approximately 1 Hz, with higher harmonics extending up to 8 Hz for root analysis. As a general guideline, frequency analysis of an ECG should at least cover a range of 0.0001–100 Hz for a normal ECG, though the fundamental frequency may be excluded from the analysis. For arrhythmogenic tendencies, spectral analysis, such as the Fourier transform, may need to extend beyond 200 Hz to capture relevant features. Further analysis is needed to determine the type of arrhythmias, requiring advanced mathematical methods to investigate the isolation and confidence levels of the specific options identified for the final diagnosis. Nonetheless, the final determination of the applicable arrhythmogenic pathology may still rest with the physician. It is important to note that extending the analysis to even higher frequencies is unlikely to yield additional diagnostic information, as the spectrum beyond this point is typically dominated by noise.

The signal processing techniques discussed here are examples of early use of AI in medical diagnostics, particularly in cardiac rhythm analysis, risk assessment, and pathological conditions screening. With advancements in knowledge, wavelet analysis has become increasingly utilized, while the matched filter approach is gaining prominence in analyzing more complex aspects of cardiac depolarization pathology.

3.4. Wavelet transform analysis

Since action potentials are mainly stochastic, wavelet analysis may not always provide the volume or quality of data required for precise diagnosis. However, when analyzing a repetitive signal as the vector summation of multiple action potentials, wavelet-domain features can effectively classify the relative contributions of higher harmonics. The wavelet features used in the analysis of an ECG signal mainly detect scaled or shifted versions of typical patterns or the aspects of depolarization wave. Wavelet decomposition using a mother wavelet that closely resembles the general shape of the QRS complex (i.e., baseline template: generic QRS complex), regardless of electrode numbering and placement, enables the

quantitative identification of the QRS complex's location, amplitude, and scaling.[29] In addition, wavelet analysis can reveal features that may not be apparent when using Daubechies and Coiflet wavelets.[34-37]

One clinically significant application of wavelet analysis is the separation of a maternal ECG from the fetal ECG during pregnancy. While the waveforms and wavelet structures of the two ECGs may share similarities, a major difference is that the fetal ECG typically has a higher repetition rate and a smaller amplitude compared to the maternal ECG. The distinct differences in the wavelet signals of fetal ECG and maternal ECG arise because the two ECG signals exist at different time and frequency scales.

3.5. Matched filter analysis

To extract maximum detail from an ECG, the optimal approach is to perform an AI-based mathematical analysis of the four-dimensional vector array derived from 12-lead data acquisition, represented in spherical coordinates:

$$\vec{v} = v(\rho, \phi, \theta, t) \quad \text{(I)}$$

This vector array is deconvolved for processing using advanced tools (Figure 5), such as the matched filter approach, which introduces a sparse multidimensional vector $\vec{w}$. In this approach, a well-defined temporal segment of the signal, representing a specific rhythm condition (template) or wavelet, is used to isolate unique depolarization events within the ECG data stream.

Biological signals, such as the ECG, are often stochastic and complex. These signals may vary rapidly due to biological and electrochemical influences. The matched filter approach can be applied to signals that lack symmetry at the zero-amplitude axis, exhibit varying repetition frequencies, or have inconsistent repeatable amplitudes over time.[37-39] The erratic signal is presumably due to chemical, mental, or physical influences, but it is not necessarily a threat or deviation from life-sustaining data streams. The matched filter approach can be used to quantify the similarity between the acquired continuous signal and a configured template, expressed by a cross-correlation coefficient that defines the match. In this way, any deviations from the template can be identified and isolated for diagnostic evaluation.

It has been shown that a small number of linear measurements of the ECG contain adequate information to reconstruct a sparse or compressible signal (i.e., compressive sensing/data acquisition).[39-41] In practice, this sparse signal will be redefined in multidimensional space. Compressive sensing is a technique for efficiently acquiring data and reconstructing signals within limits by facilitating data reduction below

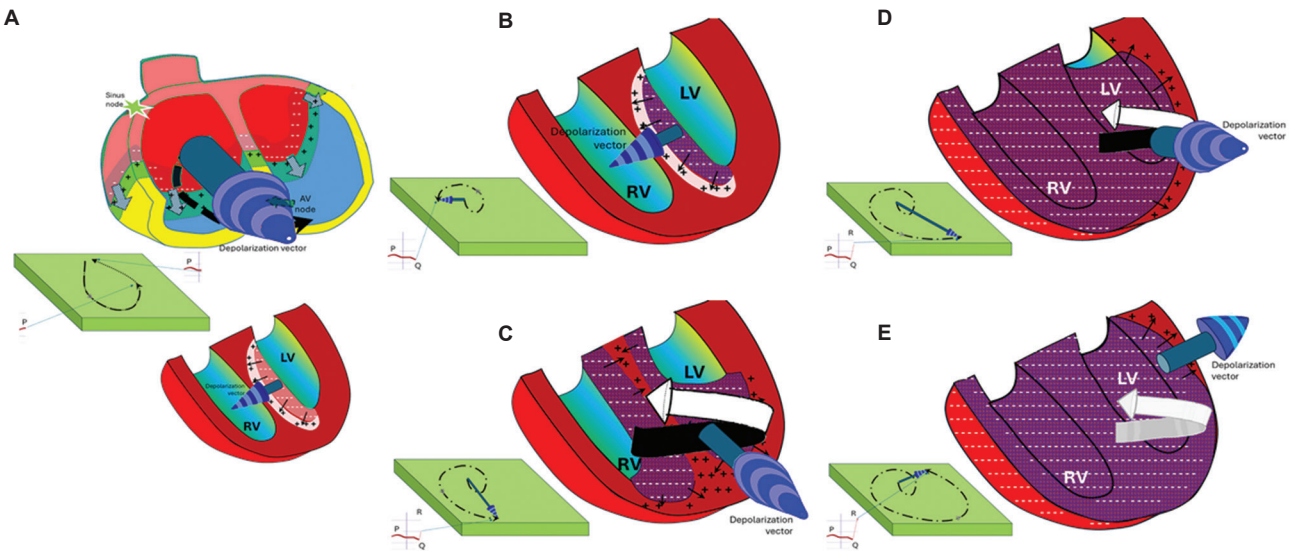

Figure 5. A three-dimensional rotating vector representing the cascading depolarization across the entire cardiac volume. (A) Initiated in the atria by a discharge from the sinus node (the natural cardiac pacemaker), represented by the P wave. (B) The onset of septal and left ventricular depolarization, originating from the passage of the excitation pulse through the Purkinje fibers to the apex of the heart, represented by the Q wave. (C) Progression into full ventricular walls illustrates the initial phases of the R wave. (D) Middle progression of the R wave. (E) Completion of the R wave depolarization front. Note that the trajectory of the rotating vector in the respective left corner is a two-dimensional projection of the full three-dimensional vector orientation as a function of time.
Abbreviations: AV: Atrioventricular; LV: left ventricle; RV: Right ventricle.

the Nyquist-Shannon sampling theorem's threshold.[10] These limits are determined through risk management by setting the accuracy, reliability, and confidence levels. For class IIb medical devices (such as important diagnostic software), these limits are set at 95% accuracy and 95% reliability. The application of compressive sensing in signal processing results in a significant reduction in computation time, offering timely updates on the patient's conditions.

Consider a J-dimensional signal vector representing the 12-lead ECG vector array (Figure 5). If this newly defined multidimensional vector has only $\varkappa$ < J non-empty components (defining a $\varkappa$-sparse signal), it can be compressed using c'$\varkappa$ linear measurements (typically, c' = 3 or 4). This J-dimensional vector now represents the inner products of the non-overlapping vectors through a set of random vectors, ultimately enabling the reconstruction of signals with high accuracy and probability. Even if the signal is not inherently sparse, it can be expressed as a sparse combination of $\varkappa$ vectors from an appropriate source.

Compressive sensing is particularly advantageous for low-complexity compression solutions, such as those involving low-bitrate signals or data-acquisition devices with low sensitivity (e.g., poorly impedance-matched skin electrodes). By computing random compressive measurements, the sensor encoder operates efficiently without requiring specific assumptions about the data stream, other than sparsity. Moreover, these measurements can be efficiently computed using analog, digital, or hybrid methods.

Given a non-uniform signal of length over time, compressive sensing can be performed on any arbitrary section of disjointed vector segments:

$$\vec{x} = \vec{v} + \vec{n} \tag{II}$$

Where $\vec{n}$ represents the noise elements in multidimensional space. For example, when

$$x_i = v_i + n_i \tag{III}$$

The arbitrary length I aims to obtain a compressed version of the acquired signal. The vector containing the acquired signal data is represented by the vector $\vec{v}$, where the length of the vector satisfies I << J, defining the compression ratio. J represents the number of signal blocks that the signal is partitioned into (signal block denoted as $\mathfrak{U}_r$), with each block having a finite length and spanning a finite time frame. The signal component v_i is scaled by a factor η_0 against a function (f_i) that is offset by a shift of ι_0, as expressed by Equation IV:

$$v_i = \eta_0 \cdot f_{i-\iota_0} \tag{IV}$$

The measured data signal vector $\vec{v}$ can be mathematically defined using *N* linear projections of the vector $\vec{w}$, with the new measurements represented as a linear combination of the original causative *M*-dimensional signal, described as:

$$\vec{v} = \Omega\vec{w} \tag{V}$$

Where Ω represents an I × J random (but identified and defined) multidimensional data matrix, typically referred to as the data acquisition sensing matrix.

Under the aforementioned conditions, with a series of J finite-length signal blocks, $\mathfrak{U}_r(\mu)$, the correlation for each segment can be computationally derived from the inner product of the signal $\mathfrak{U}_r$ with the appropriately defined vector $\varphi_n(\tau)$, as a function of time τ. The non-zero component of this inner product (also referred to as scalar product or dot product) represents the respective QRS complex. The matched filter approach provides an expression that represents the conditions of the R wave aspect through estimation in the compressed domain:

$$\varphi_n\left(\mathbb{R}_{\mathfrak{U}\varphi}(\tau) = \vec{v}, \varphi_\tau\right) \tag{VI}$$

The indices in Equation VI represent the respective signal amplitude extremes (primarily R, followed by P and T), which are to be eliminated and are used to determine the time instance $\theta_{\chi i}$. The chevrons denote the inner product. The time instance provides the basis for calculating the number of events per time frame, such as beats per minute in an ECG.

The ECG signal is ideally acquired through 12 electrodes placed on the chest, with $\mathfrak{U}_r(\tau)$ representing a recording acquired over a time interval *T* long enough to include at least one QRS complex (one single heartbeat), expressed as:

$$\mathfrak{U}_r(\tau) = \mathfrak{U}(\tau) + \mathcal{R}(\tau) = \sum_i \left\{\alpha_i \varphi(\tau - \theta_{\chi i}) + r(\tau)\right\} \tag{VII}$$

Where α_i represents the amplitude and $\theta_{\chi i}$ represents the center of a given signal kernel. The kernel encompasses the QRS complex of the individual heartbeat in the ECG signal. An additional consideration for noise contributions is represented by $r(\tau)$, as a function of time τ. This noise includes deviations from the QRS template due to transition resistance between the skin and the recording electrode(s), as well as the distorting influences of the P and T waves on the signal definition and peak detection. The heart rate is determined based on the R peak in the QRS complex

and the respective duration between sequential R peaks. The heart rate is subsequently calculated by counting the number of R peaks over a duration of 60 s.

Under the compressive sensing method described above, the one-pulse ECG signal, $\mathfrak{U}_r(\tau)$, is transformed into a J-dimensional vector:

$$\overrightarrow{\mathfrak{U}_r}(\tau) = \vec{\mathfrak{U}} + \vec{\tau} \quad \text{(VIII)}$$

While incorporating several random measurements acquired during the recording, represented by:

$$\vec{y} = \Phi\vec{\mathfrak{U}} + \vec{\tau} \quad \text{(IX)}$$

Where $\vec{y}$ falls in the domain $\vec{y} \in \Re^{\mathbb{J}}$, while $\vec{\tau}$ identifies the compressed noise and random signal influences based on the measurement and skin preparation techniques. The solution involves calculating the position $\theta_{\chi i}$ of the R-wave peak in the acquired signal using the information embedded in $\vec{y}$ for the short compressive sensing of the signal.

Based on the conditions of operating with only compressive measurements, the data do not allow for pre-processing, such as removing other signal components (e.g., the P and T waves in the ECG) or artifacts like baseline drift. Furthermore, it is not a common practice to perform pre-processing within the compressive sensing sensor. Mathematical operations are designed to account for all deviations, allowing them to be processed appropriately.

The matched filter approach will effectively determine the relevant depolarization peak. With an appropriate choice of signal template, the signal-to-noise ratio can be significantly enhanced without pre-processing. However, the variability in biological data poses a significant risk of false positives or false negatives when applying a healthy or pathological template to compressive sensing signal analysis.

In the QRS complex, the matched filter approach is used in compressive sensing to locate and determine its magnitude, based on an appropriately defined filter. This is done by performing compressive matched filtering on a relatively small number of random frequency-domain samples. In this approach, the data stream measurements are considered projections under the application of a random sensing matrix. The complete signal can subsequently be reconstructed using the results obtained from the compressive sensing approach.

To determine the correlation [$R_{x\varphi}(\tau)$] between the compressed template and the compressed cardiac muscle depolarization pattern [expressed as $\mathfrak{U}_r(\tau)$], white noise is introduced, and samples are taken with a time constant $\theta_{\chi i}$, as defined in Equation V. This time constant is determined by searching for local maxima using the matched filter approach.[35,38,39]

The QRS complex can now be expressed in the compressed domain using Equation X. The solution to the signal data stream measurements, as defined by:

$$\vec{w} = \Omega\vec{v} \quad \text{(X)}$$

Can be derived using direct estimators. The associated correlation $R_{x\psi}(n)$ can be assessed by using the direct estimator ($\breve{\mathbb{R}}_{\mathfrak{U}\varphi}$) through matrix multiplication, where $\Omega\varphi_n$ is decomposed in terms of its rows, using:

$$\vartheta_n = \vec{w}, \overrightarrow{\Omega\varphi_n} \quad \text{(XI)}$$

Hence, the correlation can be obtained:

$$\breve{\mathbb{R}}_{\mathfrak{U}\varphi} = \left[\vartheta_1, \vartheta_2, \vartheta_3, \ldots, \vartheta_{n-1}, \vartheta_n\right] \quad \text{(XII)}$$

The scalar products, or dot products, in Equations XI and XII, involve vectors of length n, illustrating the degree of alignment between the respective vectors. This does not directly require the reconstruction of the measured signal. Alternatively, the use of the orthogonalized estimator ($\breve{\mathbb{R}}_{x\varphi n}$) is often more relevant, as it is calculated by the averaged matrix product, denoted by the chevrons in the following:

$$\breve{\mathbb{R}}_{x\varphi n} = \frac{\mathbb{J}}{\mathbb{I}}\vec{w}.\left(\Omega\Omega^T\right)^{-1}\Omega\varphi_n \quad \text{(XIII)}$$

The baseline drift can be compensated for by subtracting the signal mean over time from each signal block before applying the direct estimator in Equation XIII. The signal mean can be estimated using an appropriately chosen symmetric multiplication vector, defined by the transposed unified vector array:

$$\mathbb{L}_m = \left[\frac{1}{\mathbb{J}}, \frac{1}{\mathbb{J}}, \frac{1}{\mathbb{J}}, \frac{1}{\mathbb{J}}, \ldots\ldots \frac{1}{\mathbb{J}}\right]^t \quad \text{(XIV)}$$

Subsequently yielding the vector average resulting from the vector product:

$$\widehat{\zeta_{\mathfrak{U}_r}} = \vec{\mathfrak{U}}_r, \overrightarrow{\mathbb{L}_{\boldsymbol{m}}} \quad \text{(XV)}$$

This orthogonal estimator ($\breve{\zeta}_{\mathfrak{U}_r}$) can be calculated by multiplying the data acquisition sensing matrix (Ω) with its transposed (Ω^T), as expressed by:

$$\breve{\zeta}_{\mathfrak{U}_r} = \vec{w}.\left(\Omega\Omega^T\right)^{-1}\Omega\mathbb{L}_m \quad \text{(XVI)}$$

Subsequently, subtracting the mean signal from the signal data stream holds:

$$\overrightarrow{w} = \vec{w} - \Omega\check{\zeta}_{\mathfrak{U}_r}\left[1,1,\ldots,1\right]^t \quad \text{(XVII)}$$

Representing the alternating signal free of drift.

Applying these matrix multiplication procedures to a healthy baseline signal will generate the template for analytical computations using the matched filter method. If the healthy signal is unavailable for the patient being investigated for pathological cardiac conditions, an alternative approach is to compute an average from a broad dataset of healthy individuals within the same boundary conditions as the patient. The more closely the boundary conditions match, the more effective the analytical template will be in the matched filter approach, helping to identify deviations within the repetitive full PQRST(U) pulse trains.

In the matched filter approach, the correlation that reveals the optimal estimates for the unknowns shift, $\vec{\xi}$ with respect to ξ_0, and the unknown scaling factor, $\vec{\eta}$ with respect to η_0, is implemented by utilizing the probing sequence or template (H^{ξ}_{-k}), defined by the dot product, or scalar product, of the two respective vectors:

$$\vec{\xi}\cdot\vec{\eta} = \arg\min_{\xi,\eta}\sum_k\left(x_k - \eta\cdot H_{\xi-k}\right)^2 = \arg\max_{\xi,\eta}\left[2\sum_k v_k H_{\xi-k} - \eta^2\sum_k H_{\xi-k}{}^2\right] \quad \text{(XVIII)}$$

It then follows the removal of noise (with an average value of 0), and the reversal of the sign of the equation, converting the minimum into a maximum. This results in a least-squares minimization within the domain of the data stream. By applying the Cauchy-Schwarz inequality, the two estimators reduce to, for the offset:

$$\vec{\xi} \le \sum_i v_i{}^2 = Constant \quad \text{(XIX)}$$

And for the scaling factor:[40-44]

$$\vec{\eta} = \frac{\sum_k v_k H_{\xi-k}}{\sum_k H_{\xi-k}{}^2} \quad \text{(XX)}$$

An estimation is introduced into the correlation between the compressed cardiac muscle depolarization signal and a compressed template (i.e., the average depolarization pattern complex in the compressed domain) using a matched filter template. The process employs the impulse response, which is equated to the temporal inversion of the root base signal description, $\phi(\tau)$. The computed output can be represented by Equation XXI:

$$T_{x\varphi}(\tau) = \sum_{\mu}\mathfrak{U}_r(\mu)\varphi(\mu-\tau) \quad \text{(XXI)}$$

In this case, the amplitude of $T_{x\varphi}(\tau)$ at specific moments in relative time (τ) directly indicates the degree of cross-correlation agreement between the template and the measured signal. The amplitude maxima are located where the match is highest.

As the data compression ratio $(1-\frac{I}{J})$ increases, the estimated matches of the cross-correlation function become more susceptible to noise. When all these steps are implemented in the signal processing pipeline for the temporal data acquisition of the 12-lead vectorial ECG signal, the continuous cross-correlation process enables the identification and isolation of matches and miss-matches within subsets of the input signal over time. These subsets can then be analytically compared against matched filters representing any of the over 30 pathological conditions related to cardiac rhythm abnormalities (Table 2). Following this, a root-cause analysis is conducted to determine the underlying electrochemical and electrophysiological factors contributing to the observed ECG deviations. These factors may include cell damage, malfunction, and congenital predisposing that disrupt normal cardiac function.

In the AI and machine learning framework, the computational processing of the ECG data stream begins with a comparison of the temporal pattern against a baseline normal ECG template (H^{ξ}_{-k}). Subsequently, the signal is compared against templates corresponding to the pathological conditions outlined in Table 2. This machine learning-driven process aims to identify the highest likelihood of a pathological match, such as a diseased left ventricle, as illustrated in Figure 6. A probability distribution is computed, summarizing the degree of agreement between the acquired signal and various templates. This distribution highlights both the interval matches and specific pathological conditions, providing a comprehensive diagnostic overview for physicians.[44-47] The physician then evaluates these findings in the context of the patient's background and may consult colleagues for a second opinion. Based on this thorough evaluation, a tailored treatment plan is developed.

4. Results and discussion

Long-term ECG recordings are often analyzed manually, relying on the expertise of a physician, typically an electrophysiologist, to identify episodes of arrhythmogenic cardiac depolarization or sequences of depolarization pulses that indicate the development or progression of a pathological cardiac condition. These findings guide

Table 2. A prospective spectrum of cardiac rhythm diagnostics and screening that can be quickly and automatically derived from an electrocardiogram

Number	Content
1	1st degree atrioventricular block
2	Atrial fibrillation
3	Atrial flutter
4	Bradycardia
5	Complete the right bundle branch block
6	Hypertrophic cardiomyopathy (also known as left ventricular hypertrophy)
7	Incomplete right bundle branch block
8	J-point
9	J-60 point
10	Left-axis deviation (Purkinje fibers)
11	Left anterior fascicular block
12	Left bundle branch block
13	Left ventricular dysfunction (defined as a left ventricular ejection fraction≤35%)
14	Low QRS voltages
15	Non-specific Intraventricular conduction disorder
16	PP interval
17	PR interval
18	PR segment
19	P wave duration
20	P top amplitude (in reference to QRS)
21	Pacing rhythm (sinoatrial node functionality)
22	Premature atrial contraction
23	Premature ventricular contraction
24	Prolongation of interval (e.g., long QT interval, ST segment duration, and PQ interval)
25	Prolongation of PR interval
26	Q wave abnormalities (e.g., duration, amplitude, deletion/reduction of the follow-on R wave.)
27	RR interval (i.e., derive heart rate)
28	Right-axis deviation
29	Right bundle branch block
30	Sinus arrhythmia
31	Sinus bradycardia
32	Sinus rhythm
33	Sinus Tachycardia
34	ST segment
35	ST–T segment
36	Supraventricular premature beats
37	TP interval
38	T wave abnormalities
39	T wave inversion
40	Ventricular premature beats
41	Ventricular fibrillation

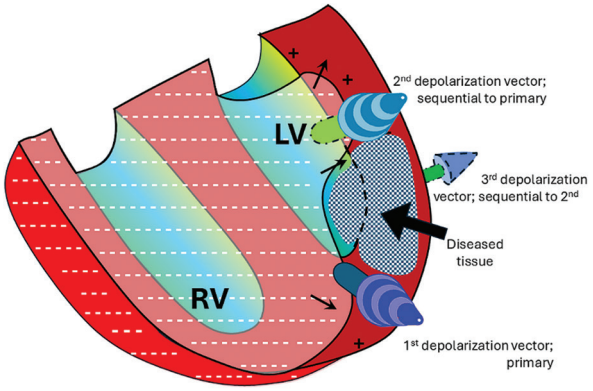

Figure 6. The infarcted volume in the left ventricular (LV) wall will cause a deformation of the R wave (as shown in Figure 7) in each recursive electrocardiogram cycle. This deformation, presenting itself as multiple conjoined peaks, a stretched peak, or other phenomena, can be detected using adaptive filter signal analysis, wavelet computational comparison, or matched filter signal processing. These methods compare the recorded signal to a healthy QRS template, as well as several other templates derived from a worldwide database of pathological and healthy electrocardiogram patterns.

the choice of treatments, which may include chemical interventions (e.g., medication), therapeutic interventions (e.g., cryoablation, alcohol ablation, and surgery), and long-term device implementation (e.g., pacemaker and implantable cardioverter defibrillator. In the worst case, the patient may require a heart transplant. These electrophysiological deviations are not age-specific. Individuals may have congenital defects that predispose them to developing pathological cardiac conditions later in life. Notably, some of these conditions can be life-threatening.

Deviations in cardiac depolarization patterns are generally classified as arrhythmias. There are numerous types of arrhythmia (as illustrated in Figure 7), each with distinct root causes and treatment options. Some of these conditions include implantation of pacemakers or implantable cardioverter defibrillators to manage or correct abnormal rhythms.

One particularly life-threatening arrhythmia is VF, which can lead to SCD if not immediately treated.[4,47-50] VF can be triggered by heart block and coronary artery disease, which is characterized by impaired perfusion and reduced oxygenation of the affected cardiac muscle cells. In cases of severe heart failure, where contractility is diminished, and intraventricular diastolic filling pressure is elevated, ventricular tachycardia can deteriorate into VF. Other life-related factors that can contribute to heart failure include:

(i) Prolonged or deep general anesthesia, for example, during extensive myocardial hypoxia or at the onset of anesthesia, especially in severely diseased patients

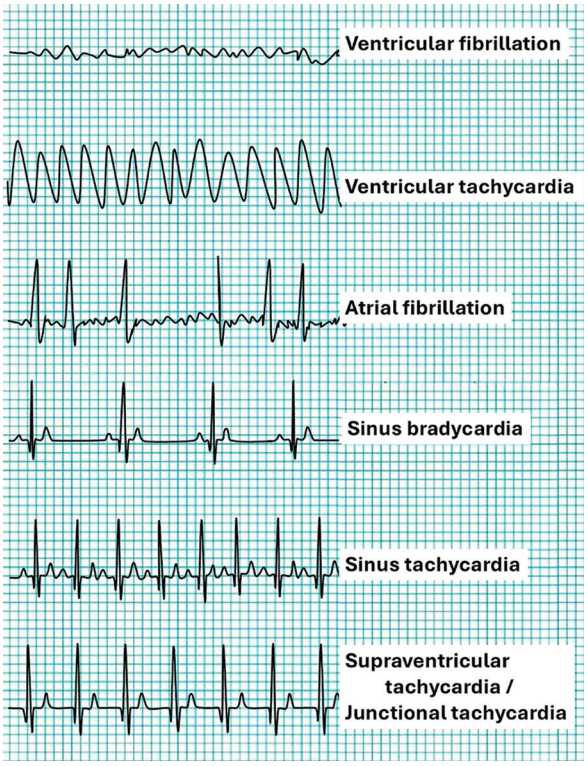

Figure 7. Representation of several characteristic electrocardiogram patterns associated with common pathological cardiac conditions

(ii) Mechanical trauma, for example, being crushed by heavy, moving participants during an American football game or other sporting events where hormonal levels are elevated
(iii) Respiratory arrest and ventilatory failure are more commonly associated with VF than primary organic cardiac disease
(iv) Many dangerous ventricular arrhythmias, which, although resembling asystole hemodynamically and electrocardiographically, are finely constructed VF.

VF is also prevalent in other mammals, including canines, felines, and equines. The most well-known dog breeds that suffer from congenital arrhythmias include the Dalmatian, Boxer, Doberman, and German Shepherd. In mammals, including humans, arrhythmias can also result from conditions like myocarditis or, more rarely, infective endocarditis (a bacterial infection of the heart valves).

A common pathological rhythm deviation observed in the frequency domain is sinus tachycardia, defined as a sinus rhythm exceeding 100 beats per minute. This condition is often due to a malfunctioning or overactive sinus node. It can also occur as a physiological response to physical exercise or psychological stress. When the sinus rhythm becomes irregular, with the longest PP or RR intervals exceeding the shortest by 0.16 seconds or more, the condition is diagnosed as sinus arrhythmia. This condition is common across all age groups but is particularly prevalent in teenagers and pre-teens, where it is sometimes not considered a pathological condition. One potential cause of sinus arrhythmia is the influence of the vagus nerve, which regulates both respiration and heart rhythm. Through the effects of the vagus nerve on the sinus node, the heart rate is increased during inspiration and decreased during expiration.

Accurate detection of fetal cardiac signals during pregnancy is critical for identifying potential congenital heart conditions. Fetal ECG recordings are obtained using leads placed in a special arrangement on the abdomen of the mother.[9] While the maternal ECG is dominant, the fetal ECG, which is superimposed on the maternal ECG, can be isolated using frequency-domain filtering. The fetal heart rate is generally higher than the maternal heart rate, enabling effective separation of the two signals using filters designed and configured in the frequency domain. Advanced frequency and wavelet analysis techniques are essential for extracting meaningful diagnostic information from these recordings.

ECG signals are stochastic and rarely perfectly reproducible. Direct analytical methods based solely on sine and cosine transformations often yield unsatisfactory results. Instead, the correlation function is typically estimated from the raw ECG data, followed by power spectrum analysis to derive frequency-domain analysis. This approach, however, is not discussed in detail in this article, as much of the verification and validation processes are proprietary.

Several frequency effects measured by the electrodes are not directly related to cardiac activity. These include noise from electrode movement, respiratory signals, and skeletal muscle activity (electromyogram). Such noise is typically filtered out in the frequency domain. A notch filter is commonly applied to eliminate frequency interference from equipment and reduce capacitive noise. Other common automated diagnostic modalities include derivation of average heart rate, peak heart rate, and low-level heart rate (e.g., recovery after exercise), as well as intervals between specific peaks in the PQRSTU complex.

More than 30 pathological cardiac rhythm deviations can now be identified using AI-driven analysis. The primary method for achieving this level of detail is 12-lead ECG monitoring over an extended period (Figure 4). The 12-lead ECG recording provides a three-dimensional view of cardiac depolarization, allowing for precise localization and characterization of abnormalities.[50-66] The approach captures the rotating depolarization vector of the heart, enabling the detection of both spatial

and temporal pathological conditions. This provides additional information beyond standard cardiac rhythm identifiers, such as heart rate and various specific interval measurements.

To isolate the true depolarization sequence, noise must be eliminated using techniques such as cutoff filtering, frequency filtering, wavelet filtering, and Wiener filtering. These methods can be applied to eliminate motion artifacts, impedance mismatches, and tissue conductivity variation.

The data acquisition device will also incorporate electronic mechanisms for signal (pre-) processing, including gain adjustment, offset correction, frequency filtering (primarily low-pass), and hardware-based automated noise reduction.[65,66] In addition, frequent and sequential repetition of deviations in the ECG pattern can be analyzed using Fourier analysis, wavelet filtering, and matched filter analysis. The wavelet, matched filter, and Wiener filtering analysis rely on an accurate base template for analysis, which must be customized to match the individual's specific history. The choice of template used for screening and diagnosis is typically based on the boundary conditions of the patient group being investigated, such as athlete status, activity level, age, gender, genetics, weight, habits, and disabilities. Women are often misdiagnosed due to the use of male-centered cardiac rhythm templates. Therefore, great care must be taken to apply the appropriate screening boundary conditions and construct a respective diagnostic template based on available prior monitoring data for the individual or a similar group. By utilizing existing data streams under healthy conditions, neural network-generated templates can be used to detect deviations and reconstruct a template that matches the suspected pathological condition through machine learning analysis.

The use of AI and deep learning techniques can be enhanced through convolutional neural network processing to provide scheduled updates, as well as to verify and validate the sampling templates used in each analytical procedure for the individual patient and their corresponding patient group selected as the baseline.[46-59] The automated ECG analysis routines currently extract the following values from the data: corrected QT interval, heart rate, P height, PQR-interval, QRS width, QT interval, R height, RR interval, and ST interval.[61]

Several verified diagnoses, as well as several desired requirements for cardiac health monitoring, are listed in Table 2. Some of these diagnostic modalities are applicable to 3-lead, 5-lead, and 12-lead ECG.[64-66] In addition, numerous diagnostic techniques are currently being developed and are in various stages of preparation for commercial release under regulatory constraints. The associated pathological conditions include but are not limited to, heart attack, arrhythmias, heart failure, cardiomyopathy, and heart valve disease. Additional diagnoses of other pathological conditions, including several rare or atypical cardiac depolarization patterns, are not listed due to their infrequent occurrence and the current limitations of the ongoing research and development program. Furthermore, many arrhythmias have yet to be investigated for AI-based discovery. For quantifiable time-specific conditions, refer to Figure 1.

5. Conclusion

Artificial intelligence-supported diagnostics offer a powerful tool for rapid patient screening and identification of cardiac abnormalities. However, a thorough investigation into the root cause of these deviations is essential to develop a comprehensive, patient-specific treatment.[65,66] The growing recognition of AI's accuracy and reliability in diagnostics is gaining widespread acceptance. In particular, AI-driven screening and risk-stratification, based on comparison with specific signal patterns of a broad range of pathological cardiac conditions, has demonstrated significant value. These tools not only improve diagnostic precision but also save time in clinical settings. Time-domain and frequency-domain filtering and analyses have long been used with excellent results. However, the introduction of more advanced techniques, such as wavelet analysis and matched filtering, has enabled the identification of complex disease patterns with higher accuracy. AI-based diagnosis can statistically determine the prevalence of certain arrhythmogenic conditions by matching ECG data with predefined templates or groups of arrhythmias. Each classification may encompass various cardiac rhythm morphologies. In addition, AI can offer details about the duration of pathological events and the frequency of specific phenomena over time, which may indicate the presence of one or more arrhythmias. The feasibility study described here provides preliminary insights into the use of AI for cardiac health screening. Nonetheless, further analysis by a physician, incorporating the patient's history and likely additional tests, will lead to a patient-specific diagnosis. Alternatively, the physician may treat the arrhythmia spectrum identified by AI as a broad-based issue, addressing it with a single, multipurpose medication.[67,68] Several drugs currently available on the market can effectively manage a wide range of cardiac rhythm problems. However, certain conditions, such as VF, cannot be controlled pharmacologically and require an implantable cardioverter defibrillator. Similarly, other arrhythmias that cannot be well-controlled by pharmaceutical means require the use of a pacemaker, as determined based on follow-up examination by the physician.[67-74]

Acknowledgments

The author wants to acknowledge the discussions with and data repository sharing by the cardiologists and electrophysiologists at the following institutions: Cleveland Clinic, Cleveland, OH, USA and London, UK, Manchester University, Manchester, UK, Cambridge University, Cambridge, UK, Havard Medical School, Cambridge, MA, USA, and University of São Paulo Medical School, São Paulo, Brazil.

Funding

None.

Conflict of interest

The author declares no conflicts of interest.

Author contributions

This is a single-authored article.

Ethics approval and consent to participate

Not applicable.

Consent for publication

Not applicable.

Availability of data

Data cannot be shared due to confidentiality concerns and proprietary analysis procedures.

References

1. Empana JP, Lerner I, Valentin E, *et al*. Incidence of Sudden cardiac death in the European Union. *J Am Coll Cardiol*. 2022;79(18):1818-1827.

   doi: 10.1016/j.jacc.2022.02.041

2. Zwietering PJ, Knottnerus JA, Rinkens PE, Kleijne MA, Gorgels AP. Arrhythmias in general practice: Diagnostic value of patient characteristics, medical history and symptoms. *Fam Pract*. 1998;15:343-353.

   doi: 10.1093/fampra/15.4.343

3. Hoefman E, Van Weert HCPM, Reisma JB, Koster RW, Bindels PJE. Diagnostic yield of patient-activated loop recorders for detecting heart rhythm abnormalities in general practice: A randomised clinical trial. *Fam Pract*. 2005;22:478-484.

   doi: 10.1093/fampra/cmi048

4. Hoefman E, Bindels PJE, Van Weert HCPM. Efficacy of diagnostic tools for detecting cardiac arrhythmias: Systemic literature search. *Neth Heart J*. 2010;18:543-551.

   doi: 10.1007/s12471-010-0831-0

5. Auer R, Bauer DC, Marques-Vidal P, Butler J, Min LJ, Cornuz J. Association of major and minor ECG abnormalities with coronary heart disease events. *JAMA*. 2012;307:1497-1505.

   doi: 10.1001/jama.2012.434

6. Mai VT, Alattas KA, Bouteraa Y, Ghaderpour E, Mohammadzadeh A. Personalized blood pressure control by machine learning for remote patient monitoring. *IEEE Access*. 2024;12:83994-84004.

   doi: 10.1109/ACCESS.2024.3413572

7. Cheng CH, Wong KW, Chin JW, Chan TT, So RHY. Deep learning methods for remote heart rate measurement: A review and future research agenda. *Sensors*. 2021;21(18):6296.

   doi: 10.3390/s21186296

8. Androulakis E, Fielder C. *Artificial Intelligence in ECG Diagnostics-where are we now*? European Society of Cardiology; 2024. Available from: https://www.escardio.org/councils/council-for-cardiology-practice-(ccp)/cardiopractice/artificial-intelligence-in-ecg-diagnostics-where-are-we-now [Last accessed on 2025 Mar 18].

9. Sau A, Pastika L, Sieliwonczyk E, *et al*. Artificial intelligence-enabled electrocardiogram for mortality and cardiovascular risk estimation: A model development and validation study. *Lancet Digit Health*. 2024;6(11):e791-e802.

   doi: 10.1016/S2589-7500(24)00172-9

10. Siontis KC, Noseworthy PA, Attia ZI, Friedman PA. Artificial intelligence-enhanced electrocardiography in cardiovascular disease management. *Nat Rev Cardiol*. 2021;18(7):465-478.

    doi: 10.1038/s41569-020-00503-2

11. Najarian K, Splinter R. *Biomedical Signal and Image Processing*. 2nd ed. Boca Raton, FL: CRC Press; 2012.

    doi: 10.1201/b11978

12. Einthoven W. Galvanometrische registratie van het menschelijk electrocardiogram [Galvanometric recording of the human electrocardiogram]. *In: Herinneringsbundel Prof. S.S. Rosenstern*. Leiden: Eduard Ijdo; 1902:101-106. (Article in Dutch)

13. Einthoven W. Het tele-cardiogram [The telecardiogram]. *Ned Tijdschr Geneeskd*. 1906;22:1517-1547. (Article in Dutch)

14. Attia ZI, Noseworthy PA, Lopez-Jimenez F, *et al*. An artificial intelligence-enabled ECG algorithm for the identification of patients with atrial fibrillation during sinus rhythm: A retrospective analysis of outcome prediction. *The Lancet*. 2019;394(10201):861-867.

    doi: 10.1016/s0140-6736(19)31721-0

15. Yusuf SW, Durand JB, Lenihan DJ, Swafford J. Dextrocardia: An incidental finding. *Tex Heart Inst J*. 2009;36(4):358-359.

16. Bernasconi A, Azancot A, Simpson JM, Jones A, Sharland GK. Fetal dextrocardia: Diagnosis and outcome in two tertiary centres. *Heart*. 2005;91(12):1590-1594.

doi: 10.1136/hrt.2004.048330

17. Garg N, Agarwal BL, Modi N, Radhakrishnan S, Sinha N. Dextrocardia: An analysis of cardiac structures in 125 patients. *Int J Cardiol*. 2003;88(2-3):143-156.

doi: 10.1016/s0167-5273(02)00539-9

18. Wiener N. *The Interpolation, Extrapolation and Smoothing of Stationary Time Series', Report of the Services 19, Research Project DIC-6037 MIT*; 1942.

19. Luengo-Fernandez R, Walli-Attaei M, Gray A, *et al*. Economic burden of cardiovascular diseases in the European Union: A population-based cost study. *Eur Heart J*. 2023;44(45):4752-4767.

doi: 10.1093/eurheartj/ehad583

20. Brown RG, Hwang PYC. *Introduction to Random Signals and Applied Kalman Filtering*. 3rd ed. New York, NY: John Wiley & Sons; 1996.

21. Welch LR. *Wiener-Hopf Theory 2006-11-25*. Available from: https://csi.usc.edu/PDF/wienerhopf.pdf [Last accessed on 2025 Mar 18].

22. Wiener N, Hopf E. *Ueber Eine Klasse Singulärer Integralgleichungen*. Berlin: Sitzungber. Akad. Wiss; 1931. p. 696-706.

23. Wiener N. *Extrapolation, Interpolation, and Smoothing of Stationary Time Series.* New York NY: John Wiley & Sons; 1949.

24. Kolmogorov AN. Stationary sequences in Hilbert space', (In Russian) Bull. *Moscow Univ*. 1941;2(6):1-40. English translation In: Kailath T, editor. *Linear Least Squares Estimation*. Stroudsburg, PA; Dowden, Hutchinson & Ross; 1977.

25. Tison GH, Zhang J, Delling FN, Deo RC. Automated and interpretable patient ECG profiles for disease detection, tracking, and discovery. *Circ Cardiovasc Qual Outcomes*. 2019;12(9):e005289.

doi: 10.1161/CIRCOUTCOMES.118.005289

26. Christopoulos G, Graff-Radford J, Lopez CL, *et al*. Artificial intelligence-electrocardiography to predict incident atrial fibrillation: A population-based study. *Circ Arrhythm Electrophysiol*. 2020;13(12):e009355.

doi: 10.1161/CIRCEP.120.009355

27. Yamashita R, Nishio M, Do RKG, Togashi K. Convolutional neural networks: An overview and application in radiology. *Insights Imaging*. 2018;9(4):611-629.

doi: 10.1007/s13244-018-0639-9

28. Rudin C. Stop explaining black box machine learning models for high stakes decisions and use interpretable models instead. *Nat Mach Intell*. 2019;1(5):206-215.

doi: 10.1038/s42256-019-0048-x

29. Ashok A, Babburi A, Ardra T, Gayathri KS, Indu RJ, Narayanan G. Performance Comparison of Matched Filter, Wavelet Denoising and Wiener Filter Technique in Communication Receivers. *In: 2018 3rd IEEE International Conference on Recent Trends in Electronics, Information and Communication Technology (RTEICT)*. IEEE; 2018:2264-2268.

doi: 10.1109/rteict42901.2018.9012318

30. Proakis JG, Manolakis DG. *Digital Signal Processing*. Available from: https://uvceee.wordpress.com/wp-content/uploads/2016/09/digital_signal_processing_principles_algorithms_and_applications_third_edition.pdf [Last accessed on 2025 Mar 18].

31. Bhattacharyya SS, Deprettere EF, Leupers R, Takala J, eds. Handbook of Signal Processing Systems. Springer International Publishing; 2019.

doi: 10.1007/978-3-319-91734-4

32. Lyons RG. *Understanding Digital Signal Processing*. Hoboken, NJ: Prentics Hall; 2010.

33. Casasent D, Chang WT. Correlation synthetic discriminant functions. *Appl Optics*. 1986;25(14):2343-2350.

doi: 10.1364/AO.25.002343

34. Holton T. *Digital Signal Processing, Principles and Applications*. Cambridge, UK: Cambridge University Press; 2021.

doi: 10.1017/9781108290050

35. Alizadehsani R, Roshanzamir M, Hussain S, *et al*. Handling of uncertainty in medical data using machine learning and probability theory techniques: a review of 30 years (1991–2020). *Ann Oper Res*. 2021;339(3):1077-1118.

doi: 10.1007/s10479-021-04006-2

36. Hannun AY, Rajpurkar P, Haghpanahi M, *et al*. Cardiologist-level arrhythmia detection and classification in ambulatory electrocardiograms using a deep neural network. *Nat Med*. 2019;25(1):65-69.

doi: 10.1038/s41591-018-0268-3

37. Turin GL. An introduction to matched filters. *IRE Trans Inform Theory*. 1960;6(3):311-332.

doi: 10.1109/TIT.1960.1057571

38. Davenpoort MA, Boufounos P, Wakin M, Baraniuk R. Signal processing with compressive measurements. *IEEE J Select Top Signal Process*. 2010;4(2):445-460.

doi: 10.1109/JSTSP.2009.2039178

39. Wimalajeewa T, Varshney PK. Sparse signal detection with compressive measurements via partial support set estimation. *IEEE Trans Signal Inform Process Over Netw*. 2017;3(1):46-60.

doi: 10.1109/TSIPN.2016.2601025

40. Fornasier M, Rauhut H. Compressive sensing. In: Scherzer O, editor. *Handbook of Mathematical Methods in Imaging*. New York, NY: Springer; 2011.

doi: 10.1007/978-0-387-92920-0_6

41. Cauchy AL. Extrait du Memoire sur quelques séries analogues à la série de lagrange, sur les fonctions symétriques et sur la formation directe des équations que produit 1'élimination des inconnues enlre des équations algébriques données [Extract from the Memoir on some series analogous to the Lagrange series, on symmetric functions and on the direct formation of equations produced by the elimination of unknowns in given algebraic equations]. *In: Oeuvres Complètes*. Cambridge University Press; 2009:73-78. [Article in French]

doi: 10.1017/cbo9780511702280.010

42. Steele JM. *The Cauchy-Schwarz Master Class: An Introduction to the Art of Mathematical Inequalities*. The Mathematical Association of America. Cambridge, UK: Cambridge University Press; 2004.

43. Steiger WL. On a generalization of the Cauchy-Schwarz in equality. *Am Math Monthly*. 1969;76:815-816.

doi: 10.1080/00029890.1969.12000339

44. Pishro-Nik H. *Introduction to Probability, Statistics, and Random Processes*. Sunderland MA: Kappa Research LLC; 2014. Available from: https://www.probabilitycourse.com [Last accessed on 2025 Mar 18].

45. Shamloo AS. Risk assessment in cardiac arrhythmias. *Eur Heart J*. 2020;41(47):4455-4457.

doi: 10.1093/eurheartj/ehaa808

46. Takase B, Ikeda T, Shimizu W, *et al.* JCS/JHRS 2022 guideline on diagnosis and risk assessment of arrhythmia. *J Arrhythm*. 2024;40(4):655-752.

doi: 10.1002/joa3.13052

47. Redfield MM, Jacobsen SJ, Burnett JC Jr., Mahoney DW, Bailey KR, Rodeheffer RJ. Burden of systolic and diastolic ventricular dysfunction in the community: Appreciating the scope of the heart failure epidemic. *JAMA*. 2003;289(2):194-202.

doi: 10.1001/jama.289.2.194

48. McDonagh TA, Metra M, Adamo M, *et al*. 2023 Focused Update of the 2021 ESC Guidelines for the diagnosis and treatment of acute and chronic heart failure. *Eur Heart J*. 2023;44(37):3627-3639.

doi: 10.1093/eurheartj/ehad195

49. Attia ZI, Kapa S, Lopez-Jimenez F, *et al*. Screening for cardiac contractile dysfunction using an artificial intelligence-enabled electrocardiogram. *Nat Med*. 2019;25(1):70-74.

doi: 10.1038/s41591-018-0240-2

50. Ribeiro AH, Ribeiro MH, Paixão GMM, *et al*. Automatic diagnosis of the 12-lead ECG using a deep neural network. *Nat Commun*. 2020;11(1):1760.

doi: 10.1038/s41467-020-15432-4

51. Rawi AA, Elbashir MK, Ahme AM. Classification of 27 heart abnormalities using 12-lead ECG signals with combined deep learning techniques. *Bull Electrical Eng Inform*. 2023;12(4):2220-2235.

doi: 10.11591/eei.v12i4.4668

52. Attia ZI, Kapa S, Yao X, *et al*. Prospective validation of a deep learning electrocardiogram algorithm for the detection of left ventricular systolic dysfunction. *J Cardiovasc Electrophysiol*. 2019;30(5):668-674.

doi: 10.1111/jce.13889

53. Kwon JM, Kim KH, Jeon KH, *et al*. Development and validation of deep-learning algorithm for electrocardiography-based heart failure identification. *Korean Circ J*. 2019;49(7):629-639.

doi: 10.4070/kcj.2018.0446

54. Cho J, Lee B, Kwon JM, *et al*. Artificial intelligence algorithm for screening heart failure with reduced ejection fraction using electrocardiography. *ASAIO J*. 2021;67(3):314-321.

doi: 10.1097/mat.0000000000001218

55. Pickham D, Zarafshar S, Sani D, Kumar N, Froelicher V. Comparison of three ECG criteria for athlete pre-participation screening. *J Electrocardiol*. 2014;47(6):769-774.

doi: 10.1016/j.jelectrocard.2014.07.019

56. Sheikh N, Papadakis M, Ghani S, *et al*. Comparison of electrocardiographic criteria for the detection of cardiac abnormalities in elite black and white athletes. *Circulation*. 2014;129(16):1637-1649.

doi: 10.1161/CIRCULATIONAHA.113.006179

57. Ko WY, Siontis KC, Attia ZI, *et al*. Detection of hypertrophic cardiomyopathy using a convolutional neural network-enabled electrocardiogram. *J Am Coll Cardiol*. 2020;75(7):722-733.

doi: 10.1016/j.jacc.2019.12.030

58. Kwon JM, Jeon KH, Kim HM, *et al*. Comparing the performance of artificial intelligence and conventional diagnosis criteria for detecting left ventricular hypertrophy using electrocardiography. *Europace*. 2020;22(3):412-419.

doi: 10.1093/europace/euz324

59. Han L, Askari M, Altman RB, *et al*. Atrial fibrillation burden signature and near-term prediction of stroke: A machine learning analysis. *Circ Cardiovasc Qual Outcomes*. 2019;12(10):e005595.

doi: 10.1161/CIRCOUTCOMES.118.005595

60. Bos JM, Attia ZI, Albert DE, Noseworthy PA, Friedman PA, Ackerman MJ. Use of artificial intelligence and deep neural networks in evaluation of patients with electrocardiographically

concealed long QT syndrome from the surface 12-lead electrocardiogram. *JAMA Cardiol*. 2021;6(5):532-538.

doi: 10.1001/jamacardio.2020.7422

61. Aufiero S, Bleijendaal H, Robyns T, *et al*. A deep learning approach identifies new ECG features in congenital long QT syndrome. *BMC Med*. 2022;20(1):162.

doi: 10.1186/s12916-022-02350-z

62. How do I analyze ECG data? Biopac Systems. Available from: https://www.biopac.com/knowledge-base/ecg-analysis/ [Last accessed on 2025 Mar 18].

63. Vahanian A, Beyersdorf F, Praz F, *et al*. 2021 ESC/EACTS guidelines for the management of valvular heart disease. *Eur Heart J*. 2022;43(7):561-632.

doi: 10.1093/eurheartj/ehab395

64. Kwon JM, Kim KH, Akkus Z, Jeon KH, Park J, Oh BH. Artificial intelligence for detecting mitral regurgitation using electrocardiography. *J Electrocardiol*. 2020;59:151-157.

doi: 10.1016/j.jelectrocard.2020.02.008

65. Elias P, Poterucha TJ, Rajaram V, *et al*. Deep learning electrocardiographic analysis for detection of left-sided valvular heart disease. *J Am Coll Cardiol*. 2022;80(6): 613-626.

doi: 10.1016/j.jacc.2022.05.029

66. Splinter R, editor. *Handbook of Physics in Medicine and Biology*. 1st ed. Baco Raton, FL: CRC Press; 2010.

doi: 10.1201/9781420075250

67. How are Arrhythmias Treated? National Heart, Lung, and Blood Institute; Updated March 24, 2022. Available from: https://www.nhlbi.nih. gov/health/arrhythmias/treatment [Last accessed on 2025 Mar 18].

68. Saljic A, Heijman J, Dobrev D. Recent advances in antiarrhythmic drug therapy. *Drugs*. 2023;83(13):1147-1160.

doi: 10.1007/s40265-023-01923-3

69. Tettey-Engmann FA, Parupelli SK, Desai SS. A review of biomedical devices: Classification, regulatory guidelines, human factors, software as a medical device, and cybersecurity. *Biomed Mater Dev Biomed Mater Dev*. 2024;2:316-341.

doi: 10.1007/s44174-023-00113-9

70. *Diagnosing Arrhythmias; Arrhythmia Alliance*. Available from: https://www.lhch.nhs.uk/media/. resources/64a7ecda3bd825.77246728.pdf [Last accessed on 2025 Mar 18].

71. Desai DS, Hajouli S. *Arrhythmias*. St. Petersburg, FL, USA: StatPearls Publishing; Updated June 5, 2023. Available from: https://www.ncbi.nlm.nih.gov/books/NBK558923 [Last accessed on 2025 Mar 18].

72. Classification of cardiac arrhythmias and conduction disturbances. *Am Heart J*. 1979;98(2):263-267.

doi: 10.1016/0002-8703(79)90230-8

73. Antzelevitch C, Burashnikov A. Overview of basic mechanisms of cardiac arrhythmia. *Card Electrophysiol Clin*. 2011;3(1):23-45.

doi: 10.1016/j.ccep.2010.10.012

74. Kiladze MR, Lyakhova UA, Lyakhov PA, Nagornov NN, Vahabi M. Multimodal neural network for recognition of cardiac arrhythmias based on 12-load electrocardiogram signals. *IEEE Access*. 2023;11:133744-133754.

doi: 10.1109/ACCESS.2023.3335176